The Compressed Hydrogen Bond in a Molecular Proton Cage

Donald B. DuPré

Department of Chemistry, University of Louisville, Louisville, Kentucky 40292

Received: May 27, 2003; In Final Form: September 24, 2003

Analysis using the theory of atoms in molecules and natural bond orbital theory of the fully optimized structure of the inside-protonated form of 1,6-diazabicyclo[4.4.4]tetradecane reveals that the encapsulated proton is engaged in a short-strong though asymmetric H-bond with covalent character. The symmetric conformer with the proton in the center of the cage was found to be a transition state with a very low barrier to proton transfer along the N···N axis. Both an implicit reaction field model (IEF−PCM) and explicit placements of chloride counterions, suggested by a published X-ray crystal structure, were found to modify the position of the proton and the strength of the H-bond. An external counterion placed along the N···N axis and near one of the bridgehead nitrogens is most effective in weakening this very hydrophobically shielded diamine H-bond. The results of this study are relevant to ongoing issues about the possible participation of unusually strong H-bonds in enzymatic catalysis.

1. Introduction

The properties, and even the existence, of strong H-bonds in condensed media remain an unresolved issue.[1−3] Experimental data and theoretically interpreted bonding patterns obtained in the gas phase that support the putative short-strong H-bond may not be applicable in solution and the solid state, where environmental factors may alter the location and dynamics of the bridging proton. This paper focuses on the properties of an encapsulated, diamine H-bond known to exist in a molecular "proton cage". Experimental X-ray and neutron diffraction data indicate that the $N_a-H^+\cdots N_b$ bond of the inside-protonated 1,6-diazabicyclo[4.4.4]tetradecane, $[4.4.4]H^+$ shown below, is symmetric (H^+ equidistant between the two nitrogens) and very short.[4−6] The central cavity of the molecule is also highly hydrophobically shielded, being surrounded by three $-(CH_2)_4-$ hydrocarbon loops with very restricted access for electrophilic attack. A representative loop will be labeled herein as N_a-(αCH_2-βCH_2-γCH_2-δCH_2)-N_b. The proton is believed to be inserted by an indirect process involving 1,2 or 1,5 transfer of an αCH_2 hydrogen.[7] Once entombed therein, H^+ cannot be removed without the destruction of the mainframe of the molecule.

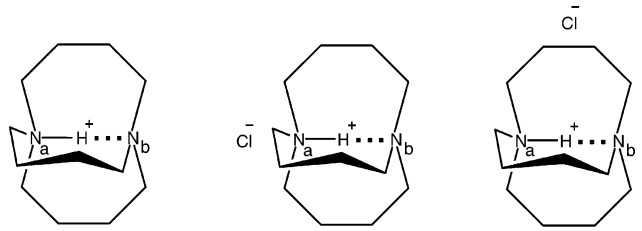

[4.4.4]H+ [4.4.4]H+Cl−

The pK_a of this extraordinary base is estimated[5,8] to be ∼25. The compound thus has a basicity orders of magnitude greater than that of more open and kinetically active proton sponges such as the prototypical 1,8-bis(dimethylamino)naphthalene (pK_a = 12.1).[5] It seems, therefore, if any molecule exhibits a short-strong H-bond that is retained in aqueous solution and the solid state, it would be $[4.4.4]H^+$. This article is a report of our studies on the free base and protonated versions of [4.4.4] in isolation and under the influence of (a) implicit solvation where the molecule is embedded in and reacts with a polarizable continuum of uniform dielectric constant and (b) explicit counterions where geometric optimizations were performed with chloride ions shown in two representative positions above. The wave function and the electron density obtained on fully optimized molecular models were analyzed with natural bond orbital (NBO) theory and the theory of atoms in molecules (AIM).

There are important implications and applications of compressed H-bonds in the field of crystal engineering[9,10] and the understanding of enzymatic catalysis.[1−3,11−20] On the latter issue, there is considerable and ongoing debate[1−3,15−20] on the importance and very existence of short-strong H-bonds.[1−3,11−20] The unusual nature of the H-bond in proton sponges is often invoked in these discussions. Briefly put, one side argues that the inherent strength of compressed H-bonds that appear to be active in the enzymatic pocket of serine proteases and other enzymes provides the necessary stabilization of the enzyme−substrate (ES) transition state. The other side, though recognizing the participation of H-bonds in catalytic function, holds that they are not exceptional. They argue that environmental effects of charged amino acid side chains and polar effects including that of competitive water molecules in the cavity will reduce the energetic importance of the H-bond. The calculations and analysis reported here address these issues in the $[4.4.4]H^+$ molecular proton cage.

2. Methods

The equilibrium and transition state geometries of the molecules of this study were fully optimized, including normal-mode frequency analysis, using density functional theory (DFT) at B3LYP/6-31+G(d,p), as implemented in Gaussian98.[21] The B3LYP exchange-correlation functional and the use of this polarized and diffuse basis set has been found to give good results for H-bonded complexes.[22] The geometric parameters obtained here are in good agreement with experimental data, where available. A few more costly calculations on $[4.4.4]H^+$ at B3LYP/6-311++G(2d,2p) (39 atoms, 628 basis functions)

10.1021/jp035476u CCC: $25.00
Published on Web 10/31/2003

showed little difference in any of the results discussed below. Simulation of environmental effects on the encapsulated $N_a-H^+\cdots N_b$ bond was performed both implicitly, with the integral equation formalism (IEF) method of the polarizable continuum solvation model (PCM) of Tomasi and co-workers,[23] and explicitly, by placement of chloride counterions in regions, shown qualitatively in the scheme above, suggested by an available X-ray crystallographic structure.[4] In the latter models, the X-ray coordinates for the initial structure with the Cl^- ion outside the cage and along the $N_a\cdots N_b$ axis had Cl^- at a distance of 4.072 Å from N_a ($\angle Cl^-N_aN_b = 180.0°$), whereas the initial structure with Cl^- perpendicular to the symmetry axis had Cl^- a distance of 4.919 Å from both nitrogens ($\angle Cl^-N_aN_b = 75.1°$). These models, as all others in this study, were fully optimized and included variations of the position of the counterion. The IEF-PCM procedure is implemented in Gaussian98 and has been found to be a convenient and reliable method for calculation of various molecular properties of solutes, as well as their geometric optimization through the use of analytical derivatives of the solvation free energies with respect to nuclear coordinates. IEF, furthermore, reduces the error in the apparent surface charge distribution as compared to the standard PCM procedure and thus provides more accurate solvation energies and geometries.

The resultant electron density from the wave function of all optimized structures was analyzed with AIM.[24,25] NBO theory was also useful in the interpretation of H-bonding in terms of local, hybrid orbital interactions more familiar to the chemist.[26−33]

In AIM, the H-bond is found to be a type of closed-shell (as opposed to shared) interaction between a donor acid (here, the hydrogen of the N_a-H^+ cation) and a base (here, the nitrogen of a tertiary amine).[24,25,34,35] As in ionic and van der Waals interactions, the electron density at the saddle point, a (3,−1) bond critical point (BCP), along the ridge of maximal density between H^+ and N_b in the H-bond is dominantly receding back into the adjacent atomic basins.[24,25] As such, it characteristically has a small value of the electron density, $\rho(r_{cp})$, at the BCP. The Laplacian, which may be written in terms of the eigenvalues of the Hesssian of ρ as $\nabla^2\rho = \lambda_1 + \lambda_2 + \lambda_3$, is also small and positive at this point in a normal H-bond.[24,25,36] The positive sign is due to the dominance ($\lambda_3 > |\lambda_1 + \lambda_2|$) of λ_3, the only positive eigenvalue whose eigenvector at the BCP points along the $N_b\cdots H^+$ bond path (BP). Covalent bonding, on the other hand, is dominated by contraction of electron density in the plane perpendicular to the bond path at the BCP ($\lambda_3 < |\lambda_1 + \lambda_2|$). The electronic charge is thus concentrated and shared between nuclei. The covalent bond is characterized by large values of $\rho(r_{cp})$ and a negative value of $\nabla^2\rho(r_{cp})$. The value of the ratio $|\lambda_1|/\lambda_3$ is also characteristic of the difference between closed shell ($|\lambda_1|/\lambda_3 < 0$) and shared ($|\lambda_1|/\lambda_3 > 0$) bonding patterns.[24,36] The local kinetic energy density per electron, $G(r_{cp})/\rho(r_{cp})$, provides another useful distinction.[36] The potential energy density, $V(r_{cp})$, is locally in excess at the BCP of a shared interaction, and consequently $G(r_{cp})/\rho(r_{cp})$ is small. Due to the retraction of charge density toward the nuclear attractors between juxtaposed closed-shell atoms, the kinetic energy dominates and $G(r_{cp})/\rho(r_{cp})$ has a relatively large value and $V(r_{cp})$ is small. Examination of the properties of the Laplacian can uncover regions of valence shell charge concentration (VSCC) where the electron density is curving inward in all directions.[24,37,38] These regions are characterized by the presence of (3,−3) critical points (CPs) where all eigenvalues λ_i of the Laplacian are negative. These CPs may or may not be directed toward bonded atoms. In the latter case, the accumulations of charge map onto the chemist's ideas of nonbonded lone pairs.[24,37,38] VSCCs may be further characterized by their spherical surface area[24] about the nucleus and thickness radially outward of the nucleus as given by μ_3, the curvature of $\nabla^2\rho$ perpendicular to the surface of this sphere.[24] A larger value of μ_3 is indicative of a thinner radial concentration of charge.

TABLE 1: Geometric Parameters of Free Base and Protonated [4.4.4] Obtained from B3LYP/6-31+G(d,p) Optimized Structures (This Work) and Experiment[4]

	[4.4.4]		[4.4.4]H^+ asym	[4.4.4]H^+ TS sym	
	free base	exptl	stationary state	transition state	[4.4.4]H^+ exptl
$N_a\cdots N_b$ (Å)	2.858	2.807	2.578	2.550	2.527
N_a-H^+ (Å)			1.152	1.275	1.263
$N_b\cdots H^+$ (Å)			1.426	1.275	
$N_a-H^+\cdots N_b$ (deg)			179.7	180.0	
sum ∠CNC (deg)[a]	347.7	346.5	339.9[b] 339.6[c]	339.0	340.8

[a] Sum of all α-carbon ∠CNC bond angles as a measure of flattening of the N bridgehead. [b] Protonated N_a. [c] H-bonded N_b.

In NBO theory, the H-bond is recognized as a general acid/base interaction, with a portion of the lone pair electron density of the base (e.g., N:) being delocalized into the $\sigma^*(A-H)$ antibonding orbital of the acidic proton donor, here $\sigma^*(N_a-H^+)$.[26−28] This interaction was assessed quantitatively in this work by use of second-order perturbation theory, where the energy lowering, $E^{(2)}$, due to the interaction of two localized orbitals a and b of energies E_a and E_b, respectively, is given by $E^{(2)} = -2\langle a|\mathbf{F}|b\rangle^2/(E_a - E_b)$, where $\langle a|\mathbf{F}|b\rangle$ is the appropriate element of the one-electron Fock or Kohn−Sham matrix.[27] Developments of NBO theory with this local orbital point of view allow the analysis of local steric interactions (e.g., lone pair repulsions) and the generation of all resonance structures with quantitative relative weights.[29−32] It is also possible to get quantitative insight about the importance, or existence, of 3-center hyperbonds.[33] We prefer the use of NBO theory over other available wave function decomposition schemes[39] due to the direct association of the underlying localized orbitals with concepts (hybrid orbitals, steric repulsion, resonance, charge transfer) familiar to and widely used by the chemist. These notions and principles are also put on a quantitative level with NBO theory. Furthermore, the method is stable to basis set extension and also does not suffer from some of the faults of others, such as violation of the Pauli principle.[26]

3. Results and Discussion

Selected geometric properties of the fully optimized structures of [4.4.4] and [4.4.4]H^+ are presented in Table 1, along with some experimental data. Tables 2−5 list essential data from the AIM analysis that we will refer to below. Some results, at the same level of theory, for small unstrained, related molecules trimethylamine (Me_3N:), trimethylammonium ion (Me_3NH^+), and the proton-bound trimethylamine dimer ($Me_6N_2H^+$) are included for purposes of comparison. The planar conformation of formamide was also examined as an extreme case of the flattening of the nitrogen base. Table 6 contains results of energetic calculations for the comparison of relative basicities of [4.4.4] in isolation and in the presence of a uniform dielectric simulating an aqueous environment.

3.1. The Free Base of [4.4.4]. There is considerable bond strain in the free base of [4.4.4] brought on by in-in, lone pair-lone pair repulsion of the bridgehead nitrogens. This causes flattening of the nitrogen bridgeheads, as conveniently measured by the sum of the angles (sum ∠CNC listed in Table 1)

TABLE 2: Properties of the Electron Density, ρ, at the Bond Critical Point (BCP) for the Free Base and Inside Protonated Forms of [4.4.4][a]

compd	A···B	$\rho(r_{cp})$	$\nabla^2\rho(r_{cp})$	r_A (au)[b]	r_B (au)[b]	$\lambda_1=\lambda_2$	λ_3	$\lvert\lambda_1\rvert/\lambda_3$	$G(r_{cp})/\rho(r_{cp})$	$V(r_{cp})$
[4.4.4]	$N_a\cdots N_b$	0.0177	0.0468	2.700	2.700	−0.0152	0.0772	0.20	0.663	−0.012
[4.4.4]H^+	N_a-H^+	0.2408	−0.9946	1.669	0.508	−0.8408	0.6870	1.22	0.290	−0.388
	$N_b\cdots H^+$	0.1191	−0.0052	1.916	0.779	−0.2878	0.5705	0.50	0.543	−0.131
[4.4.4]H^+ TS	N_a-H^+	0.1750	−0.3884	1.778	0.632	−0.5127	0.6369	0.80	0.418	−0.243
	$N_b\cdots H^+$	0.1752	−0.3900	1.777	0.632	−0.5135	0.6370	0.81	0.418	−0.244
$Me_6N_2H^+$	$N-H^+$	0.2706	−1.3179	1.629	0.466	−1.0247	0.7315	1.40	0.194	−0.435
	$N\cdots H^+$	0.0683	0.0894	2.147	0.976	−0.1271	0.3435	0.37	0.537	−0.051

[a] All values are in atomic units (au). Results for the unconstrained proton-bound trimethylamine dimer are included for comparison. AIM calculations with wave functions from fully optimized geometries obtained at B3LYP/6-31+G(d,p). [b] r_A and r_B are the distances of the BCP to atoms A and B, respectively, as identified in the second column.

TABLE 3: Properties of the Valence Shell Charge Concentrations (VSCC) of Nitrogens Obtained from an Analysis of the Laplacian, $\nabla^2\rho$, of the Electronic Charge Density

compd	VSCC location	ρ (au)	$\nabla^2\rho$ (au)	distance to N (au)	μ_3	surface area (Å^2)
[4.4.4]	in cage[a]	0.5999	−3.2606	0.729	253.3	0.73
	outside cage[b]	0.5045	−2.0283	0.753	185.8	
[4.4.4]H^+	N_a-H^+ bond	0.5653	−2.8848	0.756	178.5	0.58
	outside cage	none				
	$N_b\cdots H^+$ bond	0.5782	−3.0348	0.741	217.0	0.67
	outside cage	0.4636	−1.4873	0.763	156.4	0.05
[4.4.4]H^+ TS	$N\cdots H^+$ bonds	0.5702	−2.9381	0.748	198.8	0.62
	outside cage	none				
Me_3N:	apex (lone pair)	0.5981	−3.2898	0.730	249.9	0.73
	in pyramid[c]	0.4680	−1.5473	0.763	158.5	0.13
Me_3N-H^+	$N-H^+$ bond	0.5198	−2.4101	0.788	119.1	0.49
	in pyramid[c]	none				
formamide	above plane[d]	0.5068	−2.0618	0.754	182.0	0.35
	below plane[d]	0.5073	−2.0696	0.753	182.4	0.35

[a] Inside cage along the $N_a\cdots N_b$ axis. [b] Outside cage along the $N_a\cdots N_b$ axis, within the pyramid formed by αC−N bonds. [c] Inside the pyramid formed by C−N bonds. [d] Above and below the molecular plane of the flat conformation of formamide.

TABLE 4: Effects of Environment on the $N_a-H^+\cdots N_b$ Bond in [4.4.4]H^+ [a]

[4.4.4]H^+	gas phase	H_2O cavity	Cl^- on side	Cl^- along N···N
$N_a\cdots N_b$ (Å)	2.578	2.582	2.578	2.649
N_a-H^+ (Å)	1.152	1.135	1.133	1.068
$N_b\cdots H^+$ (Å)	1.426	1.447	1.445	1.581
∠NHN	179.7°	179.9°	179.2°	179.9°
$Cl^-\cdots N_a$ (Å)			4.224	3.459
$Cl^-\cdots N_b$ (Å)			4.408	6.107
$Cl^-\cdots H^+$ (Å)			4.107	4.527
$\angle ClN_aN_b$			76.6°	180.0°
N_a-H^+				
$\rho(r_{cp})$ (au)	0.2408	0.2520	0.2532	0.3037
$\nabla^2\rho(r_{cp})$ (au)	−0.9946	−1.0900	−1.0984	−1.5180
$N_b\cdots H^+$				
$\rho(r_{cp})$ (au)	0.1191	0.1126	0.1130	0.0802
$\nabla^2\rho(r_{cp})$ (au)	−0.0052	0.0263	0.0262	0.1174

[a] In one approach, the molecule was optimized in a fitted water cavity by using the IEF-PCM model (dielectric constant = 78.4). Alternatively, the fully optimized structure of two explicit configurations of Cl^- counterions, one on the side and the other along the $N_a\cdots N_b$ axis near the H-bonded bridgehead nitrogen, was studied with use of B3LYP/6-31+G(d,p).

subtended to each nitrogen by the adjacent α-carbons. The value of 360° would correspond to a totally flat bridgehead. The calculated value of this sum is 347.7° for the free base, which compares well with the experimental result of 346.5°.

Natural steric analysis[29] is useful here as this procedure retrieves the part of orbital interactions that is due to Pauli exchange repulsion, wherein the pressure against electrons

TABLE 5: Charge Redistribution (in Millielectrons) Due to Axial Cl^- Perturbation of the Stationary State of [4.4.4]H^+ [a]

	N_a	αC	βC	γC	δC	N_b
Cl^- effect[b]	δ^-	δ^-	δ^-	δ^-	δ^+	δ^-
charge change[c]	−3.47	−27.1	−0.556	−1.04	+18.8	−3.20
both hydrogens of $-CH_2-$ in each loop		+79.0	−25.8	−35.9	−39.3	

[a] The effect is shown in the H-bond region and in one representative hydrocarbon loop of the diazabicyclotetradecane. This loop is designated as N_a-(αCH_2-βCH_2-γCH_2-δCH_2)-N_b. [b] Increase, δ^-, or decrease, δ^+, in negative charge due to Cl^- perturbation. [c] Charge change on the heavy atom indicated. Charge change on the following: each αCH hydrogen that points toward the Cl^- ion = +92.6; H^+ = −9.30; Cl^- = +125.

TABLE 6: Total Electronic Energy, *E*, Enthalpy, *H*, Zero-Point Vibrational Energy, ZPVE, Dipole Moment, μ, and Proton Affinity, PA, for Calculated Gas-Phase and IEF-PCM (Dielectric Constant = 78.4) Models of [4.4.4] and [4.4.4]H^+ [a] **with Use of B3LYP/6-31+G(d,p)**

	gas phase		aqueous IEF-PCM	
	[4.4.4]	[4.4.4]H^+	[4.4.4]	[4.4.4]H^+
E	−581.243388	−581.672015	−581.247428	−581.745720
ZPVE	222.0	231.5	221.4	230.7
H	−580.875391	−581.289349	−580.880453	−581.364237
μ	0.002	1.094	0.016	1.758
PA[b] = $-\Delta H$	250.2		294.2	

[a] *E* and *H* are in hartrees. ZPVE and PA are in kcal/mol. μ is in D [b] PA, defined as minus ΔH of the protonation process [4.4.4] + H^+ → [4.4.4]H^+ (asymmetric stationary state), has been corrected for ZPVE and finite temperature (0−298 K).

crowding into the same spatial region is quantified by the energy of orthogonalization as pre-NBOs develop antisymmetrization tails. We find that the overlap integral of the nitrogen lone pairs is 0.067, giving rise to a contribution to the steric exchange energy in the molecule of 1.95 kcal/mol. The AIM interatomic surface (IAS) between the nitrogens is very flat and contains a (3,−1) CP connecting the nuclear attractors. Characteristic of a closed-shell interaction, the values of $\rho(r_{cp})$ and $\nabla^2\rho(r_{cp})$ (see Table 2) at this point are small and $\nabla^2\rho$ is positive. The local kinetic energy per electron here is relatively large (see typical values in Table 7.5 of Bader's book[24]), with $G(r_{cp})/\rho(r_{cp})$ = 0.663, indicating also that the electron density is receding into the atomic basins of the impinging nitrogens. The potential energy density $V(r_{cp})$ at this BCP, however, is slightly greater than $G(r_{cp})$ and thus slightly dominates the interaction by -1.75×10^{-5} au. There is some confusion[8,38,40,41] about the meaning of a BP and BCP in the electronic density between atoms engaged in what are usually regarded as repulsive interactions. Bader[38] has argued persuasively that a BP and BCP unequivocally defines a bonding, not repulsive, interaction for an equilibrium geometry. A bond may be shared or closed-shell interaction, and the later case includes what we interpret as ionic,

van der Waals, and H-bonding bonds. There is no repulsion in the equilibrium condition. Otherwise, there would be net Hellmann−Feynman forces on the nuclei and the atoms would move. This is what happens as the [4.4.4] molecule, as initially prepared, moves toward equilibrium in the calculation of the optimal geometry. During preequilibrium, there are repulsive forces, largely due to the nitrogen lone pairs, that guide the molecule down the potential energy surface to a stationary state where the net force on all nuclei is zero.

Concerning the nitrogen lone pairs in [4.4.4], the Laplacian of ρ reveals two VSCCs on each nitrogen, oriented along the $N_a\cdots N_b$ axis: one inside the cage, one outside. The spherical surface area of each inside VSCC represents a lone pair like charge accumulation that is relatively large (0.73 Å^2), and the same as that found for isolated trimethylamine (Me_3N:) at the same level of theory (Table 3). This indicates, as pointed out already in the study of Howard et al.,[8] that there is nothing exceptional about the electronic density about the nitrogens in this proton cage that can account for extraordinary basicity. The appearance of the second (3,−3) CP associated with each nitrogen outside the cage, along the $N_a\cdots N_b$ axis and within the pyramid formed by the planes of the three αC−N bonds, is a consequence of the flattening of the bridgeheads. Such a CP is not found for NH_3 in its equilibrium conformation. An inner-pyramid (3,−3) CP emerges, however, in the process of the umbrella inversion of NH_3 as the amine becomes planar.[42] It is noteworthy here that our reference free amine Me_3N: also exhibits a second VSCC within the C−N bond pyramid at equilibrium (see Table 3). This indicates that steric repulsion of the methyl groups forces sufficient flattening of the amine to produce an additional (3,−3) CP along the symmetry axis. NBO analysis shows that the nitrogen lone pairs of [4.4.4] have substantial p-character (93% in a state of $sp^{12.4}$ hybridization). The presence of the two VSCCs along the $N_a\cdots N_b$ axis thus is suggestive of the two lobes of the p-function on either side of each nitrogen nucleus. Dual, nonbonded VSCCs about nitrogen were also noted in the planar formamide molecule.[42,43] At the level of theory of the calculations reported in this paper, the two out-of-plane VSCCs of nitrogen in formamide are equivalent, but not collinear, subtending an angle of 163.7° about the nitrogen nucleus (Table 3). According to NBO theory, the formamide nitrogen lone pair has 100% p-character. The NBO lone pair of Me_3N: has less p-character (85%, $sp^{5.8}$). The inner-cage, nonbonded VSCC of each nitrogen in [4.4.4] is the thinnest of all amines/amides studied here, with the largest value of the radial curvature (μ_3 = 253.3 au) along the $N_a\cdots N_b$ axis. The latter property does suggest some compression of the nitrogen electronic density along $N_a\cdots N_b$ in the free base of [4.4.4].

3.2. Stationary State and Transition State for Proton Transfer across the Cage in [4.4.4]H$^+$. X-ray data[4] show that the $N_a\cdots N_b$ distance in this diazabicyclotetradecane contracts from 2.807 Å to 2.527 Å upon inside protonation and the H-bond is symmetric, with both N to H^+ bond lengths of 1.263 Å (see Table 1). $\Delta\delta(^1H,D)$ NMR data also support the symmetry of this bond.[44−45] Our DFT calculations at the B3LYP/6-31+G-(d,p) level reproduce these experimental values very nicely, but show that the symmetrically H-bonded conformer is actually a transition state, lying at the top of a very low, 0.18 kcal/mol high, barrier straddling a double minimum on the potential energy surface. When accounting for zero-point vibrational energy corrections, this theoretical barrier effectively disappears, reconciling the theoretical picture with the experimental data. The unimpeded proton is simply moving too fast from side to side of the cage to be captured in the time window of these experimental methods. Previous theoretical work on this molecule did not discuss the dynamics of the proton transfer, perhaps because, with those Hartree−Fock optimizations, the symmetric protonated [4.4.4]H$^+$ was not recognized to be a transition state.[8,46]

The framework of the cage also relaxes upon protonation. The bridgehead nitrogens, in particular, are less flattened with the sum of ∠CNC bond angles decreasing by about 8° on going from 347.7° in the free base to 339.9°/339.6° (asymmetric stationary state) and 339.0° (transition state) upon protonation (see Table 1). As a reference for comparison, we also present our results, at the same level of theory, on the optimization of the $Me_6N_2H^+$ dimer. The H-bond in this unfettered diamine has a longer N···N separation (2.761 Å), a shorter covalent N_a−H^+ bond (1.108 Å), and a weaker $N_b\cdots H^+$ bond (1.652 Å). The ∠CNC sum about the protonated nitrogen in the dimer is 333.9°, somewhat flatter than the H-bonded one with 330.2°. The corresponding values of this index for the isolated monomers are almost the same, with 334.3° for Me_3N: and 335.4° for Me_3NH^+. The larger difference in nitrogen pyramidalization in the bound dimer relates to charge transfer from the tail of the amine into the head of the donor acid, reducing electrostatic repulsion of the methyl groups on the basic side. The much smaller difference (only 0.3°) in bridgehead flattening in the [4.4.4]H$^+$ stationary state is a consequence of the equalization of the compressed N to H^+ bonds, and relaxation of charge differences of like atoms in similar positions across the proton cage. Little is changed in the latter regard with the movement of the proton to the center of the cage in forming the transition state.

Our AIM analysis of the compressed H-bond in [4.4.4]H$^+$ shows that $\rho(r_{cp})$ at the BCP on the N_a−H^+ side is relatively large and the Laplacian is negative (see Table 2). The ratio $|\lambda_1|/\lambda_3 = 1.22$ is typical of a covalent bond, as is the small value of the local kinetic energy per electron, $G(r_{cp})/\rho(r_{cp}) = 0.290$. The corresponding properties of the BCP on the $N_b\cdots H^+$ side also demonstrates covalent nature: $\rho(r_{cp}) = 0.1191$ au is small, but the Laplacian is slightly *negative*, $\nabla^2\rho(r_{cp}) = -0.0052$ au. The values of $|\lambda_1|/\lambda_3 = 0.50$ and $G(r_{cp})/\rho(r_{cp}) = 0.543$ at the BCP of the H-bond are intermediate between those found for typical covalent and H-bonds (see again, for example, Table 7.5 of Bader's book[24]). The positioning of the two BCPs of the bridging hydrogen is asymmetric, the IAS being extended more toward the acceptor nitrogen N_b (see data in Table 2 and Figure 1). Further examination of the Laplacian about the H-bonding region revealed that the BCP of the electron density of the weaker $N_b\cdots H^+$ interaction lies on the nodal surface ($\nabla^2\rho = 0$) enveloping the N_a−H^+ covalent bond as shown in Figure 1. This is characteristic of an interaction intermediate between the shared and the closed shell.[24] The H-bonded nitrogen is also seen to be strongly polarized toward the proton (estimated nitrogen axial asymmetry ratio in this direction of 1.7) and is clearly close to the formation of a continuous envelope of shared electron density across the cage. This merger is fulfilled in the transition state, Figure 2 and Table 2, where the proton is covalently bound to both nitrogens, with $\rho(r_{cp}) = 0.1750$ and 0.1752 au, and $\nabla^2\rho(r_{cp}) = -0.3884$ and −0.3900 au, respectively.

In the stationary state, the H-bonded nitrogen of [4.4.4]H$^+$ retains the two VSCCs discussed above for each nitrogen of the free base (see Table 3). The inner-cage charge accumulation has a smaller spherical surface area (0.67 Å^2 vs 0.73 Å^2), and is radially thicker (μ_3 = 217.0 au vs 253.3 au) and further away from N_b. The outer (3,−3) CP of the nitrogen on the protonated

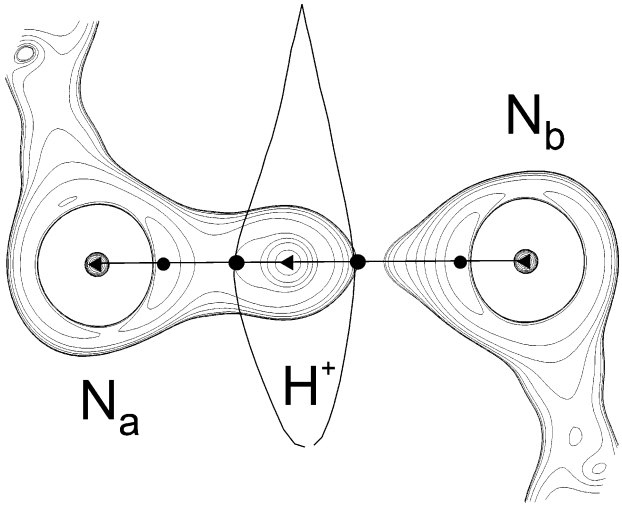

Figure 1. Contour plot of the Laplacian of the electron density showing regions of charge concentration about the asymmetric, though slightly covalent, $N_a-H^+\cdots N_b$ hydrogen bond in the stationary state of [4.4.4]-H^+. Lines of charge depletion are not included for purposes of clarity. Filled triangles are the sites of the nuclear attractors in the order of $N_a-H^+\cdots N_b$ from left to right; small solid circles are the (3,−3) critical points of the valence shell charge concentration (VSCC) of both nitrogens; the larger solid circles are the (3,−1) bond critical points of the electron density itself. The two vertical curves passing through the latter points show where the interatomic surface separating the proton and the two bonded nitrogen atoms cuts the plane of this diagram.

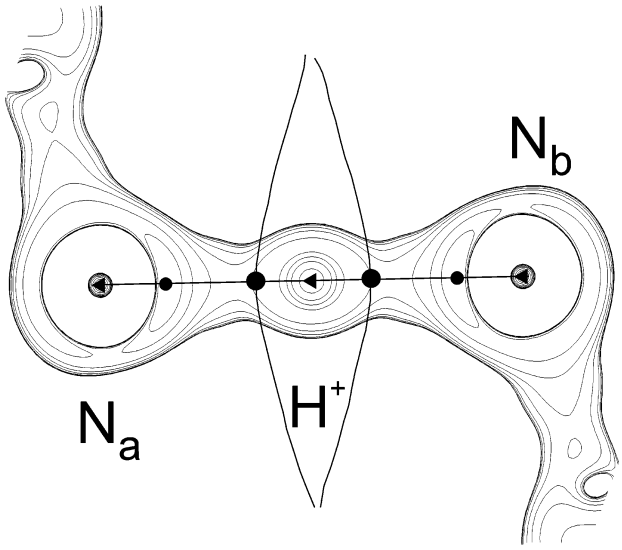

Figure 2. Contour plot of the Laplacian of the electron density showing regions of charge concentration about the symmetric transition state for proton transfer in $[4.4.4]H^+$. Symbols have the same meaning as in Figure 1.

side has disappeared. The latter is also true in the transition state, where we see that both nitrogens share the proton in a covalent manner.

NBO theory offers an alternative interpretation of the $N_a-H^+\cdots N_b$ bond based on localized orbitals. Calculations within this theoretical framework show a strong, partial delocalization of the nitrogen lone pair, $n(N_b)$, into the $\sigma^*(N_a-H^+)$ antibond, amounting to $E^{(2)}$ values of 91 kcal/mol for the stationary state and 159 kcal/mol for the transition state. Note that these values are not the absolute H-bond strengths. There are also repulsions among these atoms due to the nuclei and almost filled bonding and nonbonding orbitals that must be considered in the total energetics of the H-bond. Nevertheless, these are very strong interactions for H-bonds and $N_a-H^+\cdots N_b$ might be considered as a 4 electron-3 centered (4e-3c) bond,[33] as in the resonance structure $N_a{:}-H^+-{:}N_b$. This proves to be the case with 3.9 electrons occupying a 3c-hyperbond, polarized 63% toward the covalent proton donor in the stationary state and symmetrical in the transition state. These results are consistent with the large values of the $n(N_b)\rightarrow\sigma^*(N_a-H^+)$ interaction cited above, the low electron occupancy found for the nitrogen lone pair orbital (1.77 in the stationary state and 1.70 in the transition state), and the high occupancy of the $\sigma^*(N_a-H^+)$ antibond (0.20 in the stationary state and 0.27 in the transition state). The dominant resonance structures for the asymmetric stationary state, found with natural resonance theory (NRT),[30−32] are $N_a-H^+\cdots{:}N_b$ and $N_a{:}\cdots H^+-N_b$, with relative weightings of 40%/22%, respectively. The weightings are approximately equal, 28%/30%, respectively, for the transition state. The proton acceptor $N_b\cdots H^+$ bond in the stationary state has a NRT bond order of 0.33, which has 22% covalent character. In the transition state, both N to H^+ bonds have bond orders of 0.44 and are 29% covalent, according to this analysis. The results from NBO analysis are thus in qualitative and semiquantitative agreement with AIM theory and offer some orbital level insight into the nature of this strong H-bond.

3.3. Effect of the Environment. The above results, obtained from both AIM and NBO at a correlated level of theory, show that the bridgehead nitrogen atoms of $[4.4.4]H^+$, in isolation, are definitely pulled together by a short and strong H-bond. What about the real environment of $[4.4.4]H^+$? Is the H-bond substantially weakened by competitive, external electrostatic effects? To answer this question, we performed two computational procedures to simulate surroundings. Our IEF-PCM,[23] self-consistent reaction-field calculations showed significant effects on the geometry of the H-bond when the molecule is placed in a fitted cavity with the dielectric constant of water. As seen in Table 4, within the dielectric the $N_a\cdots N_b$ distance is increased by 0.004 Å, the N_a-H^+ bond is shortened by 0.017 Å, and the $N_b\cdots H^+$ bond is elongated by a like amount, 0.021 Å. The electron density at the BCP of the $N_b\cdots H^+$ bond falls and $\nabla^2\rho(r_{cp})$ becomes slightly positive. These changes are more significant than they might appear as bond order is generally found to scale exponentially with the value of $\rho(r_{cp})$.[24,25] (No functional expressions are available that relate $\rho(r_{cp})$ for $N_b\cdots H^+$ H-bonds to bond order.) Very similar effects on the H-bond were observed for the fully optimized DFT structure of $[4.4.4]H^+Cl^-$ with an explicit Cl^- counterion placed outside the cage and perpendicular to the $N_a\cdots N_b$ axis (see the structures in the Introduction). The counterion pulls H^+ toward the protonated nitrogen in both cases studied for $[4.4.4]H^+Cl^-$. However, when the Cl^- ion is placed along the $N_a\cdots N_b$ axis and near the N_a bridgehead nitrogen, the perturbation is more substantial (Table 4). Here the $N_a\cdots N_b$ distance is increased by 0.071 Å, the N_a-H^+ bond is shortened by 0.084 Å, and the $N_b\cdots H^+$ bond is elongated by 0.155 Å, as compared to the gas-phase calculations. The $\angle NH^+N$ angle remains linear. The weakening of the H-bond is also reflected in the loss of electron density at the BCP and the larger and more positive value of $\nabla^2\rho(r_{cp})$. The latter properties are actually closer to those found for the unconstrained H-bond in the isolated $Me_6N_2H^+$ dimer (see Table 2) where the H-bond is also linear and the nitrogens are 0.113 Å further apart (2.761 Å in the dimer vs 2.649 Å in $[4.4.4]H^+Cl^-$). Solvation effects on H-bond strength in even this very shielded proton cage thus can matter, particularly for special, explicit placements of counterions.

Figure 3 is an illustration of the effect of an axially placed chloride ion on the $N_a-H^+\cdots N_b$ H-bond. The BCP of the IAS

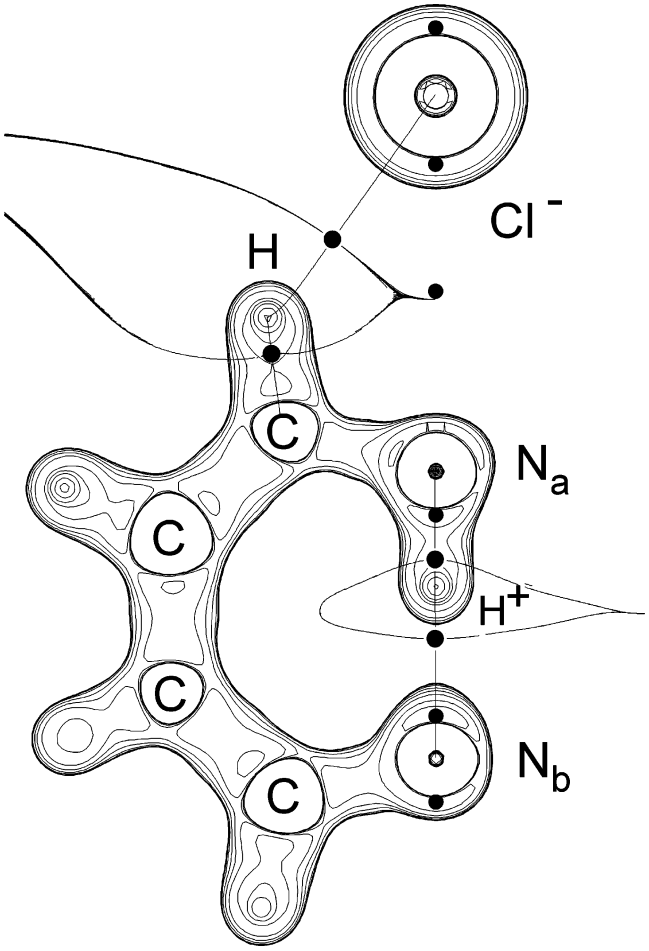

Figure 3. Contour plot of the Laplacian of the electron density showing the effect of a chloride counterion placed outside the cage along the $N_a\cdots N_b$ axis and near the N_a bridgehead nitrogen. The plane of this diagram includes Cl^-, N_a, N_b, H^+, and one of the αCH_2 hydrogens on one of the hydrocarbon loops that is pointed toward Cl^- and exhibits a bonding interaction with it. Small solid circles are (3,−3) critical points of charge concentrations; the larger solid circles are the (3,−1) bond critical points of the electron density itself. The interatomic surface (IAS) of the αC−H hydrogen is also shown. The BCP of the αC−H bond is, however, slightly out of plane. All of the carbon atoms and other hydrogens of the loop are out of plane. Note the difference in the IAS of H^+ here and in Figure 1: the BCP of the $N_b\cdots H^+$ bond has moved away from the nodal surface of the Laplacian envelope ($\nabla^2\rho = 0$) about the N_a-H^+ covalent bond and is similar in placement to that in a normal H-bond.

between H^+ and N_b is no longer coincident with the nodal surface of the envelope of the Laplacian about the N_a-H^+ covalent bond as in Figure 1, and is more characteristic of a normal H-bond than the intermediate interaction discussed above for isolated $[4.4.4]H^+$. This BCP is now in a region of charge depletion and $\nabla^2\rho(r_{cp})$ is thus positive. N_b is also less polarized toward N_a-H^+. Bond paths also exist in the electron density connecting the anion to three α-carbon hydrogens that point toward Cl^-. One of these α-methylene hydrogen interactions is shown in Figure 3. The electron density at the indicated BCP is rather small, with $\rho = 0.0145$ and $\nabla^2\rho(r_{cp}) = 0.0441$. This is a weak ionic interaction. There is no bond path between Cl^- and N_a, but a (3,−3) CP is found on this axis. The value of $\rho = 0.0080$ at this point, however, is very small.

The charge transfer between Cl^- in the axial position and the proton cage was also studied through the calculation of atomic charges obtained by integration over the atomic basins of the atoms listed in Table 5 and Table S1 (included in the Supporting Information). The results include the time-consuming integrations for one representative hydrocarbon loop. The chloride ion loses 125 millielectrons (me) to the cage. The H-bond is affected by an increase in negative charge on both nitrogens and the bridging hydrogen, but the effect is small with a 3.47 me increase on N_a, 3.20 me on N_b, and 9.30 me on H^+. A substantial amount of electron density, 92.6 me, is removed from each αCH hydrogen that points directly toward Cl^-. This is expected on the basis of exclusion repulsion between the valence shell of Cl^- and the bordering hydrogens. The α-carbon takes on a substantial amount, 27.1 me, of the ion-transferred and cage-redistributed charge, whereas the β- and γ-carbons are much less affected. The δ-carbon nearest N_b, however, becomes more positive by 18.8 me, as it presumably transfers electron density to its bonded methylene hydrogens and, to a lesser extent, to the more electronegative N_b. The charge transferred from the axial chloride ion is seen to be borne primarily by the α-carbons and the methylene hydrogens of the hydrocarbon loops—other than the αCH hydrogens that are in contact with Cl^- and loose electron density.

Some insight into the nature of the influence of environmental factors on the basicity of [4.4.4] can also be obtained from calculations of the proton affinity (PA). Table 6 shows the results of such calculations, comparing the gas-phase protonation energies and enthalpies with those under the influence of the uniform aqueous dielectric. The PA, defined as minus ΔH of the protonation process[47] $[4.4.4] + H^+ \rightarrow [4.4.4]H^+$ (asymmetric stationary state), has been corrected for zero-point vibrational energy (ZPVE) and finite temperature (0−298 K). The gas-phase result of PA = 250.2 kcal/mol is in good agreement with the estimate of Howard et al.[8] As a reference point, this value is about 10 kcal/mol greater than that calculated[47] for tetramethylquanidine—one of the strongest neutral, organic superbases. In the presence of the simulated aqueous medium, the value for $[4.4.4]H^+$ rises to 294.2 kcal/mol. The medium, with a dielectric constant of 78.4, results in a larger PA even though the H-bond is reduced in strength as evidenced by the larger $N_a\cdots N_b$ and $N_b\cdots H^+$ bond distances and the reduction in $\rho(r_{cp})$ and the change in sign of $\nabla^2\rho(r_{cp})$ at the BCP of the H-bond. The larger stabilization of the $[4.4.4]H^+$ cation in an aqueous-like, polar medium relative to the gas phase is a reflection of the greater charge separation realized for the asymmetric molecular structure in the polarized continuum optimization. The dipole moment of $[4.4.4]H^+$ is 1.758 D for the PCM structure, but only 1.094 D for the molecule (asymmetric stationary state) in isolation. It is noted that the medium also slightly stabilizes the free base through solute polarization.

4. Conclusions

Using the theory of atoms in molecules (AIM) and natural bond orbital (NBO) analysis, with full geometric optimizations at correlated levels of computation, we find that the H-bond in $[4.4.4]H^+$ in isolation is indeed strong with covalent properties. In our calculations, the symmetric version of $[4.4.4]H^+$ with the proton in the center of the cage was found to be a transition state with a very low barrier to proton transfer. The H-bond is weakened by environmental effects, simulated by the presence of a uniform polarizable continuum with the dielectric constant of water and explicit placements about the cage of chloride counterions. Our results on the $[4.4.4]H^+Cl^-$ proton cage model show that an inherently strong and well-protected H-bond may be reduced to relatively normal behavior by the influence of explicitly placed negative charges some distance away. The perturbation is particularly effective when Cl^- is placed near a

bridgehead nitrogen along the $N_a \cdots N_b$ axis. The message is brought to the H-bond in part through a polarization of the electronic structure of the intermediate hydrocarbon region. Most of the charge transferred from the anion is, however, borne by the α-carbons and the methylene hydrogens, with the exception of the αCH hydrogens that point toward and share an IAS with Cl^-. The IEF-PCM optimized model exhibits a larger proton affinity than the gas-phase result, even though the H-bond is weaker. Environmental factors considered, the primary influence of the H-bond in relieving the bond strain of the cage remains. The role of the compressed H-bond in this type of strain relief may be a crucial source of the catalytic effect in certain enzymes. The primary influence may be not in the strength of the H-bond, but in the reduction of lone pair repulsion on nitrogen and oxygen atoms within the preorganized and polarized mainframe of the enzymatic pocket that holds the substrate. Counter to this is the previously established cooperative influence in certain cases where explicitly placed water molecules have been found theoretically to *increase* the strength of a H-bond.[48,49] What is actually going on in enzymatic catalysis must depend on the details of the architectural arrangement of charged and polar species within the ES pocket, and may involve compressed, though weakened, H-bonds.

Acknowledgment. Supercomputer time allocations received from the National Computational Science Alliance under grants CHE98008N, CHE990012N, and CHE020031 and from the Advanced Biomedical Computing Center of the Frederick Cancer Research and Development Center, National Institutes of Health are acknowledged. Support for this work also came from a Research Initiation Grant from the Office of the Vice President for Research, University of Louisville. Helpful discussions with Dr. Igor Vorobyov are also acknowledged.

Supporting Information Available: Tables of the coordinates of the optimized free base and protonated versions of [4.4.4] and AIM atomic charges discussed in this article. This material is available free of charge via the Internet at http://pubs.acs.org.

References and Notes

(1) Gerlt, J. A.; Kreevoy, M. M.; Cleland, W. W.; Frey, P. A. *Chem. Biol.* **1997**, *4*, 259.
(2) Guthrie, J. P. *Chem. Biol*. **1996,** *3*, 163.
(3) Chen, J.; McAllister, M. A.; Lee, J. K.; Houk, K. N. *J. Org. Chem.* **1998**, *63*, 4611.
(4) Alder, R. W.; Orpen, A. G.; Sessions, R. B. *J. Chem. Soc., Chem. Commun.* **1983**, 999.
(5) Alder, R. W.; Eastman, P.; Hext, N. M.; Moss, R. E.; Orpen, A. G.; White, J. M. *J. Chem. Soc., Chem. Commun.* **1988**, 1528.
(6) Alder, R. W.; Moss, R. E.; Sessions, R. R. *J. Chem. Soc., Chem. Commun.* **1983**, 997.
(7) Alder, R. W.; Casson, A.; Sessions, R. B. *J. Am. Chem. Soc.* **1979**, *101*, 3652.
(8) Howard, S. T.; Platts, J. A.; Alder, R. W. *J. Org. Chem.* **1995**, *60*, 6085.
(9) Desiraju, G. R. *Chem. Commun.* **1997**, 1475.
(10) Aakeroy, C. B. *Acta Crystallogr.* **1997**, *B53*, 569.
(11) Cleland, W. W.; Kreevoy, M. M. *Science* **1994**, *264*, 1887.
(12) Warshel, A.; Papazyan, A.; Kollman, P. A. *Science* **1995**, *269*, 102.
(13) Cleland, W. W.; Kreevoy, M. M. *Science* **1995**, *269*, 104.
(14) Frey, P. A. *Science* **1995**, *264*, 104.
(15) Kim, K. S.; Oh, K. S.; Lee, J. Y. *Proc. Natl. Acad. Sci. U.S.A.* **2000**, *97*, 6373.
(16) Perrin, C. L.; Nielson, J. B. *Annu. Rev. Phys. Chem.* **1997**, *48*, 511.
(17) Kim, K. S.; Kim, D.; Lee, J. Y.; Tarakeshwar, P. K.; Oh, S. *Biochemistry* **2002**, *41*, 5300.
(18) Viragh, C.; Harris, T. K.: Reddy, P. M.; Massiah, M. A.; Mildvan, A. S.; Kovach, I. M. *Biochemistry* **2000**, *39*, 16200.
(19) Westler, W. M.; Frey, P. A.; Lin, J.; Wemmer, D. E.; Morimoto, H.; Williams, P. G.; Markey, J. L. *J. Am. Chem., Soc. Commun.* **2002**, *124*, 4196.
(20) Perrin, C. L.; Ohta, B. K. *J. Am. Chem. Soc.* **2001**, *123*, 6520.
(21) Frisch, M. J.; Trucks, G. W.; Schlegel, H. B.; Scuseria, G. E.; Robb, M. A.; Cheeseman, J. R.; Zakrzewski, V. G.; Montgomery, J. A., Jr.; Stratmann, R. E.; Burant, J. C.; Dapprich, S.; Millam, J. M.; Daniels, A. D.; Kudin, K. N.; Strain, M. C.; Farkas, O.; Tomasi, J.; Barone, V.; Cossi, M.; Cammi, R.; Mennucci, B.; Pomelli, C.; Adamo, C.; Clifford, S.; Ochterski, J.; Petersson, G. A.; Ayala, P. Y.; Cui, Q.; Morokuma, K.; Salvador, P. J.; Dannenberg, J.; Malick, D. K.; Rabuck, A. D.; Raghavachari, K.; Foresman, J. B.; Cioslowski, J.; Ortiz, J. V.; Baboul, A. G.; Stefanov, B. B.; Liu, G.; Liashenko, A.; Piskorz, P.; Komaromi, I.; Gomperts, R.; Martin, R. L.; Fox, D. J.; Keith, T.; Al-Laham, M. A.; Peng, C. Y.; Nanayakkara, A.; Challacombe, M.; Gill, P. M. W.; Johnson, B.; Chen, W.; Wong, M. W.; Andres, J. L.; Gonzalez, C.; Head-Gordon, M.; Replogle, E. S.; Pople, J. A. *Gaussian 98*, Revision A.11; Gaussian, Inc.: Pittsburgh, PA, 2001.
(22) Del Bene, J. E.; Person, W. B.; Szczepaniak, K. *J. Phys. Chem.* **1995**, *99*, 10705.
(23) Cances, E.; Mennucci, B.; Tomasi, J. *J. Chem. Phys.* **1997**, *107*, 3032.
(24) Bader, R. F. W. *Atoms in Molecules. A Quantum Theory*; Clarendon Press: Oxford, UK, 1990.
(25) Popelier, P. *Atoms in Molecules. An Introduction*; Prentice Hall: New York, 2000.
(26) Reed, A. E.; Curtiss, L. A.; Weinhold, F. *Chem. Rev.* **1988**, *88*, 899.
(27) Weinhold, F. Natural Bond Orbital Methods. in *The Encyclopedia of Computational Chemistry*; Schleyer, P. v. R., Editor-in-Chief; John Wiley & Sons: Chichester, UK, 1998.
(28) Reed, A. E.; Weinhold, F.; Curtiss, L. A.; Pochatko, D. J. *J. Chem. Phys.* **1986**, *84*, 5687.
(29) Badenhoop, J. K.; Weinhold, F. *J. Chem. Phys.* **1997**, *107*, 5406.
(30) Glendening, E. D.; Weinhold, F. *J. Comput. Chem.* **1998**, *19*, 593.
(31) Glendening, E. D.; Badenhoop, J. K.; Weinhold, F. *J. Comput. Chem.* **1998**, *19*, 610.
(32) Glendening, E. D.; Weinhold, F. *J. Comput. Chem.* **1998**, *19*, 628.
(33) Weinhold, F.; et al. *NBO 5.0 Program Manual. Natural Bond Orbital Analysis Programs*, NBO 5.0; Theoretical Chemistry Institute, University of Wisconsin: Madison, WI, 2001.
(34) Carroll, M. T.; Chang, C.; Bader, R. F. W. *Mol. Phys.* **1988**, *63*, 387.
(35) Koch, U.; Popelier, P. L. A. *J. Phys. Chem.* **1995**, *99*, 9747.
(36) Bader, R. F. W.; Essén, H. *J. Chem. Phys.* **1984**, *80*, 1943.
(37) Bader, R. F. W.; MacDougall, P. J.; Lau, C. D. H. *J. Am. Chem. Soc.* **1984**, *106*, 1594.
(38) Bader, R. F. W. *J. Phys. Chem.* A **1998**, *102*, 7314.
(39) Kitaura, K.; Morokuma, K. *Int. J. Quanum Chem.* **1976**, *10*, 325.
(40) Cioslowski, J.; Mixon, S. T. *Can. J. Chem.* **1992**, *70*, 443.
(41) Cioslowski, J.; Edgington, L.; Stefanov, B. B. *J. Am. Chem. Soc.* **1995**, *117*, 10381.
(42) Malcolm, N. O. J.; Popelier, P. L. A. *J. Phys. Chem. A* **2001**, *105*, 7638.
(43) Laidig, K. E.; Bader, R. F. W. *J. Am. Chem. Soc.* **1991**, *113*, 6312.
(44) Alder, R. W.; Orpen, A. G.; Sessions, R. B. *J. Chem. Soc., Chem. Commun*. **1983**, 1000.
(45) Gunnarsson, G.; Wennerstrom, H.; Egan, W.; Forsen, S. *Chem. Phys. Lett*. **1976**, *38*, 96.
(46) Howard, S. T. *J. Am. Chem. Soc*. **2000**, *122*, 8238.
(47) Koppel, I. A.; Schwesinger, R.; Breuer, T.; Burk, P.; Herodes, K.; Koppel, I.; Leito, I.; Mishima, M. *J. Phys. Chem. A* **2001**, *105*, 9575.
(48) Go, H.; Karplus, M. *J. Phys. Chem.* **1994**, *98*, 7104.
(49) Kumar, G. A.; Pan, Y.; Smallwood, C. J.; McAllister, M. A. *J. Comput. Chem*. **1998**, *19*, 1345.